

The Dependence of Galaxy Shape on Luminosity and Surface Brightness Profile

R. Anthony Vincent

Department of Physics, The Ohio State University, Columbus, OH 43210

vincent.59@osu.edu

and

Barbara S. Ryden

Department of Astronomy, The Ohio State University, Columbus, OH 43210

ryden@astronomy.ohio-state.edu

ABSTRACT

For a sample of 96,951 galaxies from the Sloan Digital Sky Survey Data Release 3, we study the distribution of apparent axis ratios as a function of r -band absolute magnitude and surface brightness profile type. We use the parameter `fracDeV` to quantify the profile type (`fracDeV` = 1 for a pure de Vaucouleurs profile; `fracDeV` = 0 for a pure exponential profile). When the apparent axis ratio q_{am} is estimated from the moments of the light distribution, the roundest galaxies are very bright ($M_r \sim -23$) de Vaucouleurs galaxies and the flattest are modestly bright ($M_r \sim -18$) exponential galaxies. When the axis ratio q_{25} is estimated from the axis ratio of the 25 mag/arcsec² isophote, we find that de Vaucouleurs galaxies, at this low surface brightness, are flatter than exponential galaxies of the same absolute magnitude. For a given surface brightness profile type, very bright galaxies are rounder, on average, than fainter galaxies. We deconvolve the distributions of apparent axis ratios to find the distribution of the intrinsic short-to-long axis ratio γ , making the assumption of constant triaxiality T . For all profile types and luminosities, the distribution of axis ratios is inconsistent with a population of oblate spheroids, but is usually consistent with a population of prolate spheroids. Bright galaxies with a de Vaucouleurs profile ($M_r \leq -21.84$, `fracDeV` > 0.9) have a distribution of q_{am} that is consistent with triaxiality in the range $0.4 \lesssim T \lesssim 0.8$, with mean axis ratio $0.66 \lesssim \langle \gamma \rangle \lesssim 0.69$. The fainter de Vaucouleurs galaxies are best fit with prolate spheroids ($T = 1$) with mean axis ratio $\langle \gamma \rangle \approx 0.51$.

Subject headings: galaxies: elliptical and lenticular, cD, galaxies: fundamental parameters, galaxies: photometry, galaxies: spiral, galaxies: statistics

1. INTRODUCTION

The galaxy classification scheme of Hubble (1926) has proved durably useful. As modified and extended by de Vaucouleurs (1959), it is still the standard method for classifying low-redshift galaxies with high surface brightness. The Hubble classification scheme was originally based on the appearance of galaxies on photographic plates. Elliptical galaxies have smooth elliptical isophotes; spiral galaxies have spiral arms that wind outward from a central bulge or bar. It was later discovered that for luminous galaxies, the surface brightness profile is strongly correlated with the Hubble type. If the surface brightness I is measured along the major axis of a galaxy’s image, it is found that bright elliptical galaxies have surface brightness profiles that are well fit by a de Vaucouleurs, or $R^{1/4}$ law, for which $\log I \propto -R^{1/4}$ (de Vaucouleurs 1948). By contrast, the azimuthally averaged surface brightness profile of a spiral galaxy, outside its central bulge, is typically well fit by an exponential law, $\log I \propto -R$ (Freeman 1970). It was also eventually realized that galaxies of different Hubble type have different kinematic properties. The disks of spiral galaxies are rotationally flattened, with stars and gas on nearly circular orbits with little random motion. Bright elliptical galaxies ($M_B \lesssim -20$), by contrast, are slowly rotating and are supported mainly by their anisotropic velocity dispersion.

One shortcoming of the Hubble classification scheme, imposed by necessity, is that elliptical galaxies are classified by their apparent two-dimensional shape, seen in projection on the sky, rather than their intrinsic three-dimensional shape. Consider an idealized galaxy whose surfaces of constant luminosity density are concentric, coaxial, similar ellipsoids, with principal axes of lengths $a \geq b \geq c$; the shape of the galaxy can then be described by the two axis ratios $\beta \equiv b/a$ and $\gamma \equiv c/a$. Equivalently, the shape can be described by the two numbers γ and T , where the triaxiality parameter T is given by the relation $T \equiv (1 - \beta^2)/(1 - \gamma^2)$. If the ellipsoidal galaxy is seen in projection, though, its isophotes will be concentric, coaxial, similar ellipses. The shape of the projected image can then be described by the single axis ratio $q \equiv B/A$, where A and B are the major and minor axis length of any isophote.

Although knowing the apparent axis ratio q is not, by itself, sufficient to determine the intrinsic axis ratios β and γ , the three-dimensional shape of galaxies is not beyond all conjecture. Two approaches to determining the three-dimensional shape of galaxies have been used. First, the intrinsic shape of an individual galaxy can be modeled if kinematic

data are available in addition to photometric data (Binney 1985; Franx, Illingworth, & de Zeeuw 1991). However, accurate galaxy modeling requires either multiple long-slit position angles (Statler 1994) or integral-field spectroscopy (Statler et al. 2004), and is best applied to systems with high surface brightness and large angular size. The second approach, which can be used in the absence of kinematic information, is to make statistical estimates of the distribution of β and γ for a large sample of galaxies. Early estimates of the intrinsic shape distribution made the assumption that elliptical galaxies were oblate spheroids, with $\beta = 1$ (Hubble 1926; Sandage, Freeman, & Stokes 1970). More recent studies, using accurate surface photometry, reveal that the distribution of apparent shapes for ellipticals cannot be explained by a population of randomly oriented oblate spheroids; it can easily be explained, however, by a population of triaxial ellipsoids (Fasano & Vio 1991; Lambas, Maddox, & Loveday 1992; Ryden 1992; Tremblay & Merritt 1995; Alam & Ryden 2002).

In this paper, we use the photometry-only approach to constraining the intrinsic shapes of galaxies, using the Sloan Digital Sky Survey Data Release 3 (SDSS DR3) as our source of galaxy photometry. Previous studies using the SDSS Early Data Release and Data Release 1 studied the axis ratios of galaxies best fit by de Vaucouleurs profiles (Alam & Ryden 2002) and those best fit by exponential profiles (Ryden 2004). In this paper, we more closely examine the relation between surface brightness profile and intrinsic shape. In addition, we determine, for each profile type, the dependence of intrinsic shape on galaxy luminosity. For elliptical galaxies, the distribution of apparent shapes is known to depend on absolute magnitude. Elliptical galaxies with $M_B \lesssim -20$ are rounder on average than fainter ellipticals (Tremblay & Merritt 1996); for a typical elliptical galaxy color of $B - V \approx 0.9$ (Roberts & Haynes 1994), the dividing luminosity corresponds to $M_V \approx -20.9$. In this paper, given the large sample size provided by the SDSS DR3, we can look for a similar shape dichotomy not only among galaxies with de Vaucouleurs profiles, but among galaxies with a variety of surface brightness profile types.

In §2 of this paper, we describe the SDSS and the methods by which we determine the apparent axis ratio of the galaxies in our sample. In §3, we examine how the apparent axis ratios depend on the galaxy profile type and the galaxy luminosity, then use nonparametric kernel estimators to determine the distribution of apparent axis ratios for different samples of galaxies, subdivided by luminosity and profile type. In §4, we invert the distribution of apparent axis ratios to find the distribution of intrinsic axis ratios, assuming galaxies all have the same triaxiality parameter T . In addition to looking at purely oblate galaxies ($T = 0$) and purely prolate galaxies ($T = 1$), we also examine the results for triaxial galaxies with $T = 0.2$, $T = 0.4$, $T = 0.6$, and $T = 0.8$. In §5, we discuss the implications of the observed galaxy shapes for different scenarios of galaxy formation and evolution.

2. DATA

The Sloan Digital Sky Survey (York et al. 2000; Stoughton et al. 2002) will, when complete, provide a map of nearly one-fourth of the celestial sphere. A CCD mosaic camera (Gunn et al. 1998) images the sky in five photometric bands (*ugriz*; Fukugita et al. (1996); Smith et al. (2002)). The Main Galaxy Sample (MGS) of the SDSS (Stoughton et al. 2002) will eventually contain $\sim 10^6$ galaxies with $r \leq 17.77$; the mean redshift of galaxies in the MGS is ~ 0.1 , determined from a follow-up spectroscopic survey. The SDSS Data Release 3, issued to the astronomical community in 2004 October, contains 5282 square degrees of imaging data and 4188 square degrees of spectroscopic data (Abazajian et al. (2005); see also Stoughton et al. (2002), Abazajian et al. (2003), and Abazajian et al. (2004)).

The SDSS DR3 data processing pipeline provides a morphological star/galaxy separation, with extended objects being classified as ‘galaxies’ and point-like objects being classified as ‘stars’. For each galaxy, in each photometric band, a pair of models are fitted to the two-dimensional galaxy image. The first model has a de Vaucouleurs surface profile (de Vaucouleurs 1948):

$$I(R) = I_e \exp\left(-7.67[(R/R_e)^{1/4} - 1]\right) , \quad (1)$$

truncated beyond $7R_e$ to go smoothly to zero at $8R_e$. The second model has an exponential profile:

$$I(R) = I_e \exp(-1.68[R/R_e - 1]) , \quad (2)$$

truncated beyond $3R_e$ to go smoothly to zero at $4R_e$. For each model, the apparent axis ratio q_m and the phase angle φ_m are assumed to be constant with radius. The parameters q_m , φ_m , R_e , and I_e are varied to give the best χ^2 fit to the galaxy image, after convolution with a double-Gaussian fit to the point spread function.

The SDSS DR3 pipeline also takes the best-fit exponential model and the best-fit de Vaucouleurs model and finds the linear combination of the two that best fits the galaxy image. The fraction of the total flux contributed by the de Vaucouleurs component is the parameter `fracDeV`, which is constrained to lie in the interval $0 \leq \text{fracDeV} \leq 1$. The `fracDeV` parameter delineates a continuum of surface brightness profile types, from the pure de Vaucouleurs (`fracDeV` = 1) to the pure exponential (`fracDeV` = 0).

The SDSS DR3 databases provide many different measures of the apparent axis ratio q of each galaxy in each of the five photometric bands. In this paper, we will use the r band data, at an effective wavelength of 6165Å. (We also repeated our analysis at g and i , the other two bands with high signal-to-noise, and did not find significantly different results from our r band analysis.) Two measures of the apparent axis ratio are given by the best-fitting axis ratios q_m for the de Vaucouleurs and exponential models. However, the algorithm for

fitting the models introduces quantization in the distribution of q_m . Because of this artificial quantization, we do not use the model axis ratios as estimates of the true apparent shapes of galaxies.

A useful measure of the apparent shape in the outer regions of galaxies is the axis ratio of the 25 mag arcsec⁻² isophote. The SDSS DR3 data pipeline finds the best fitting ellipse to the 25 mag arcsec⁻² isophote in each band; the semimajor axis and semiminor axis of this isophotal ellipse are A_{25} and B_{25} . The isophotal axis ratio $q_{25} \equiv B_{25}/A_{25}$ then provides a measure of the apparent galaxy shape at a few times the effective radius. For galaxies in our sample with `fracDev` = 1, the mean and standard deviation of A_{25}/R_e are 3.12 ± 1.00 ; for galaxies with `fracDev` = 0, the mean and standard deviation are $A_{25}/R_e = 2.40 \pm 0.36$.

Another measure of the apparent shape is q_{am} , the axis ratio determined by the use of adaptive moments of the galaxy’s light. The method of adaptive moments determines the n th order moments of a galaxy image, using an elliptical weight function whose shape matches that of the image (Bernstein & Jarvis 2002; Hirata & Seljak 2003). The SDSS DR3 adaptive moments use a weight function $w(x, y)$ that is a Gaussian matched to the size and ellipticity of the galaxy image $I(x, y)$. The adaptive first order moments,

$$x_0 = \frac{\int xw(x, y)I(x, y)dxdy}{\int w(x, y)I(x, y)dxdy} \quad (3)$$

and

$$y_0 = \frac{\int yw(x, y)I(x, y)dxdy}{\int w(x, y)I(x, y)dxdy} \quad (4)$$

tell us the ‘center of light’ of the galaxy’s image. With this knowledge, we can compute the adaptive second order moments:

$$M_{xx} = \frac{\int (x - x_0)^2 w(x, y)I(x, y)dxdy}{\int w(x, y)I(x, y)dxdy} \quad (5)$$

and so forth. The SDSS DR3 provides for each image the values of the parameters $\tau = M_{xx} + M_{yy}$, $e_+ = (M_{xx} - M_{yy})/\tau$, and $e_\times = 2M_{xy}/\tau$. The adaptive second moments can be converted into an axis ratio using the relation

$$q_{\text{am}} = \left(\frac{1 - e}{1 + e} \right)^{1/2} \quad (6)$$

where $e = (e_+^2 + e_\times^2)^{1/2}$.

The adaptive moments axis ratio q_{am} , computed in the manner given above, is not corrected for the effects of seeing. The SDSS DR3 also provides the fourth order adaptive moments of the galaxy image, and the adaptive moments τ_{psf} , $e_{+, \text{psf}}$, and $e_{\times, \text{psf}}$ of the

point spread function at the galaxy’s location. These moments can be used to correct for the smearing and shearing due to seeing; such corrections are essential for studying the small shape changes resulting from weak lensing (Bernstein & Jarvis 2002; Hirata & Seljak 2003). However, in this paper we will only look at well-resolved galaxies for which the seeing corrections are negligibly small.

Our full sample of galaxies consists of those objects in the SDSS DR3 spectroscopic sample which are flagged as galaxies and which have spectroscopic redshifts $z > 0.004$ (to eliminate contaminating foreground objects) and $z < 0.12$ (to reduce the possibility of weak lensing significantly distorting the observed shape). To ensure that galaxies were well resolved, we also required $\tau > 7\tau_{\text{psf}}$. The absolute magnitude M_r of each galaxy was computed from the Petrosian r magnitude and the spectroscopic redshift, assuming a Hubble constant $H_0 = 70 \text{ km s}^{-1} \text{ Mpc}^{-1}$ in a flat universe with $\Omega_{\text{m},0} = 0.3$ and $\Omega_{\Lambda,0} = 0.7$. No K-correction was applied to the data; for galaxies with normal colors at low redshift the K-correction in the r band is small – less than 0.2 mag for an average elliptical galaxy at $z = 0.12$, and even less for galaxies at smaller redshifts or with bluer colors (Fukugita, Shimasaku, & Ichikawa 1995).

The total number of galaxies in our full sample, selected in this way, is $N_{\text{gal}} = 96,951$. Of the full sample, only 919 galaxies have $\text{fracDeV} = 1$, and 26,994 have $\text{fracDeV} = 0$. The remainder, constituting 71% of the full sample, are best fit by a combination of a de Vaucouleurs and exponential model, with $0 < \text{fracDeV} < 1$.

3. APPARENT SHAPES

It remains to be demonstrated that fracDeV is a useful parameter for describing the surface brightness profile type of galaxies. After all, a linear combination of the best de Vaucouleurs fit and the best exponential fit will not, in general, be the best possible de Vaucouleurs plus exponential fit. An alternative method of describing surface brightness profiles is by fitting a Sérsic profile (Sérsic 1968):

$$\log I \propto -(R/R_e)^{1/n} , \tag{7}$$

where n can be an arbitrary number. This fitting method was used, for instance, by Blanton et al. (2003) in their study of SDSS galaxies. If, in fact, galaxies are well described by Sérsic profiles, then fracDeV is a useful surrogate for the Sérsic index n . Consider, for instance, a galaxy whose surface brightness is perfectly described by a Sérsic profile of index $n = 2$ and effective radius $R_e = X$. The best-fitting exponential model for this galaxy (fitting in the radial region $0.1X \leq R \leq 10X$) has $R_e = 1.10X$; the best-fitting de Vaucouleurs model

has $R_e = 0.80X$. Combining the models gives $\text{fracDeV} = 0.51$ for this $n = 2$ Sérsic galaxy. A similar fit to an $n = 3$ Sérsic galaxy yields $\text{fracDeV} = 0.83$. In general, if galaxies have Sérsic profiles with $1 \leq n \leq 4$, then fracDeV , as computed by the SDSS DR3 pipeline, is a monotonically increasing function of the Sérsic index n , and thus can be used as a surrogate for n .

A plot of the mean axis ratio $\langle q \rangle$ as a function of the parameter fracDeV is shown in Figure 1. The mean adaptive moments axis ratio $\langle q_{\text{am}} \rangle$, indicated by the filled circles, shows an increasing trend with fracDeV , from $\langle q_{\text{am}} \rangle = 0.59$ for galaxies with purely exponential profiles ($\text{fracDeV} = 0$) to $\langle q_{\text{am}} \rangle = 0.74$ for galaxies with pure de Vaucouleurs profiles ($\text{fracDeV} = 1$). However, the trend in $\langle q \rangle$ is not a linear one; for galaxies with $\text{fracDeV} \lesssim 0.5$, the value of $\langle q \rangle$ is nearly constant at $\langle q \rangle \approx 0.6$; it is only at $\text{fracDeV} \gtrsim 0.5$ that $\langle q \rangle$ shows an increasing trend with fracDeV . The mean isophotal axis ratio $\langle q_{25} \rangle$, indicated by the open circles in Figure 1, shows less of a trend with fracDeV . Except in the case of nearly pure de Vaucouleurs profiles ($\text{fracDeV} \gtrsim 0.9$), the axis ratio of a galaxy in its outer regions doesn't seem to depend on its surface brightness profile.

For convenience in analysis, we have divided our galaxy sample into four classes, based on the value of fracDeV . Galaxies with $\text{fracDeV} \leq 0.1$, corresponding to a Sérsic index $n \lesssim 1.2$, are called ‘ex’ galaxies; there are $N_{\text{ex}} = 44,289$ ‘ex’ galaxies in our sample. Galaxies with $0.1 < \text{fracDeV} \leq 0.5$, corresponding to $1.2 \lesssim n \lesssim 2.0$, are labeled ‘ex/de’ galaxies ($N_{\text{ex/de}} = 36,645$). Galaxies with $0.5 < \text{fracDeV} \leq 0.9$, corresponding to $2.0 \lesssim n \lesssim 3.3$, are labeled ‘de/ex’ galaxies ($N_{\text{de/ex}} = 13,780$). Finally, galaxies with $\text{fracDeV} > 0.9$, corresponding to $n \gtrsim 3.3$, are called ‘de’ galaxies. The small fraction of ‘de’ galaxies in our sample ($N_{\text{de}} = 2237$) is partly due to the fact that the centrally concentrated de Vaucouleurs galaxies are less likely to satisfy our resolution criterion, and partly due to the fact that galaxies with high Sérsic indices are intrinsically rare; Blanton et al. (2003) estimated that only $\sim 5\%$ of the SDSS galaxies in their sample had Sérsic index $n > 3$.

The ‘de’ galaxies are rounder in their central regions than in their outer regions: $\langle q_{\text{am}} - q_{25} \rangle = 0.083$. This is consistent with the ‘de’ galaxies being relatively bright elliptical galaxies, for which the isophotal axis ratios tend to decrease with increasing semimajor axis length (Ryden, Forbes, & Terlevich 2001). By contrast, the ‘ex’ galaxies are actually slightly flatter in their central regions than in their outer regions: $\langle q_{\text{am}} - q_{25} \rangle = -0.017$.

For a given surface brightness profile type, there exists a relation between absolute magnitude and apparent axis ratio. Contour plots of mean apparent axis ratio as a function of both fracDeV and M_r are given in Figure 2. (To give a feel for the absolute magnitude scale, fitting a Schechter function to the luminosity function of SDSS galaxies yields $M_{*,r} \approx -21.4$ (Nakamura et al. 2003).) The upper panel of the figure shows that the trend in $\langle q_{\text{am}} \rangle$ runs

from the flattest galaxies at $\text{fracDeV} \approx 0$ and $M_r \approx -18$, where $\langle q_{\text{am}} \rangle \approx 0.52$, to the roundest galaxies at $\text{fracDeV} \approx 1$ and $M_r \approx -23$, where $\langle q_{\text{am}} \rangle \approx 0.83$. This result is not surprising, since moderately bright galaxies with exponential profiles are intrinsically flattened disk galaxies, while extremely bright galaxies with de Vaucouleurs profiles are intrinsically nearly spherical giant elliptical galaxies (Tremblay & Merritt 1996). More surprising are the results shown in the bottom panel of Figure 2, which shows $\langle q_{25} \rangle$, the mean isophotal axis ratio. Here, we find that the apparently flattest galaxies, as measured by q_{25} , are not exponential galaxies, but galaxies with $\text{fracDeV} \approx 0.7$ (corresponding to Sérsic index $n \approx 2.5$) and $M_r \approx -20.5$; these galaxies have $\langle q_{25} \rangle \approx 0.53$. The roundest galaxies, measured by $\langle q_{25} \rangle$, are not bright de Vaucouleurs galaxies, but bright exponential galaxies; the maximum value of $\langle q_{25} \rangle$ is ≈ 0.74 , at $\text{fracDeV} \approx 0$, $M_r \approx -22.5$. Note also that for bright galaxies ($M_r \lesssim -21$), the contours of constant $\langle q_{25} \rangle$ in Figure 2 are nearly horizontal. That is, among bright galaxies, the flattening of the outer isophotes doesn’t depend strongly on the surface brightness profile type.

A view of the dependence of $\langle q \rangle$ on absolute magnitude for each of our four profile types, ‘ex’, ‘ex/de’, ‘de/ex’, and ‘de’, is given in Figure 3. In the upper panel, which shows $\langle q_{\text{am}} \rangle$, note that for each profile type, there is a critical absolute magnitude M_{crit} at which $\langle q_{\text{am}} \rangle$ is at a minimum. This critical absolute magnitude ranges from $M_{\text{crit}} \sim -20.6$ for the ‘de’ galaxies to $M_{\text{crit}} \sim -19.4$ for the ‘ex’ galaxies. At $M_r < M_{\text{crit}}$, the value of $\langle q_{\text{am}} \rangle$ increases relatively rapidly with increasing luminosity; at $M_r > M_{\text{crit}}$, the value of $\langle q_{\text{am}} \rangle$ increases less rapidly with decreasing luminosity. At a fixed absolute magnitude, the average axis ratio of ‘de’ galaxies is always greater than that of ‘ex’ galaxies; however, for $M_r \lesssim -20$, the flattest galaxies, on average, at a given absolute magnitude are not the ‘ex’ galaxies, but those with the mixed ‘de/ex’ and ‘ex/de’ profile types. The bottom panel of Figure 3 shows $\langle q_{25} \rangle$ versus M_r for the different profile types. In the interval $-20 \lesssim M_r \lesssim -22$, we see that ‘ex’ galaxies have *larger* values of $\langle q_{25} \rangle$ than galaxies of other profile types.

Tremblay & Merritt (1996) divided elliptical galaxies into two classes; galaxies brighter than $M_B \approx -20$ are rounder on average than fainter ellipticals. Using a typical color for elliptical galaxies of $B - V \approx 0.9$, this corresponds to an absolute magnitude in the r band of $M_r \approx -21.2$, using the transformation $r = B - 1.44(B - V) + 0.12$ (Smith et al. 2002). In our data, we do not see an abrupt jump in $\langle q_{\text{am}} \rangle$ for ‘de’ galaxies at $M_r = -21.2$, but rather a more gradual increase between $M_r \approx -20.6$ and $M_r \approx -22.7$. In addition, it is true for any profile type that highly luminous galaxies are rounder, on average, than less luminous galaxies.

Knowing the mean shape as a function of M_r for each profile type (‘de’, ‘de/ex’, ‘ex/de’, ‘ex’) does not tell us the complete distribution of axis ratios, $f(q)$. In order to compare the

distribution of axis ratios for highly luminous galaxies with that for less luminous galaxies, we determined, for each profile type, the dividing absolute magnitude M_0 such that the distribution $f(q_{\text{am}})$ for galaxies with $M_r \leq M_0$ is maximally different from the distribution $f(q_{\text{am}})$ for galaxies with $M_r > M_0$. We measure the difference between the distributions by applying a Kolmogorov-Smirnov (K-S) test, and finding the value of M_0 that minimizes the K-S probability P_{KS} . The values of the dividing magnitude M_0 for each profile type, and the associated probability P_{KS} , are given in Table 1. (Using a Student’s t-test for the significance of the difference of the means yields similar values of M_0 , differing by less than 0.2 mag from the values found using the K-S test.)

To estimate the distribution of apparent axis ratios $f(q)$ for each of our galaxy subsamples, we use a nonparametric kernel technique (Vio et al. 1994; Tremblay & Merritt 1995; Ryden 1996). Given a sample of N axis ratios, q_1, q_2, \dots, q_N , the kernel estimate of the frequency distribution $f(q)$ is

$$\hat{f}(q) = \frac{1}{N} \sum_{i=1}^N \frac{1}{h_i} K\left(\frac{q - q_i}{h_i}\right), \quad (8)$$

where $K(x)$ is the kernel function, normalized so that

$$\int_{-\infty}^{\infty} K(x) dx = 1. \quad (9)$$

To ensure that our estimate \hat{f} is smooth, we use a Gaussian kernel, with $K(x) \propto \exp(-x^2/2)$. The parameter h_i in equation (8) is the kernel width; too small a width introduces noise into the estimate, while too great a kernel width produces excessive smoothing. We choose the kernel width h_i by using the standard adaptive two-stage estimator of Abramson (1982). In this technique, an initial estimate \hat{f}_0 is made using a global fixed kernel width

$$h = 0.9A/N^{0.2}, \quad (10)$$

with $A = \min(\sigma, Q_4/1.34)$, where σ is the standard deviation and Q_4 is the interquartile range of the axis ratios. For samples that are not strongly skewed, this formula minimizes the mean square error (Silverman 1986; Vio et al. 1994). The final estimate \hat{f} is then computed, using at each data point q_i the kernel width

$$h_i = h \left[G/\hat{f}_0(q_i) \right]^{1/2}, \quad (11)$$

where G is the geometric mean of \hat{f}_0 over all values of i .

The axis ratio for a galaxy must lie in the range $0 \leq q \leq 1$. To ensure that $\hat{f} = 0$ for $q < 0$ and $q > 1$, we impose reflective boundary conditions at $q = 0$ and $q = 1$. In practice,

this means replacing the simple Gaussian kernel with the kernel

$$K_{\text{ref}} = K\left(\frac{q - q_i}{h_i}\right) + K\left(\frac{-q - q_i}{h_i}\right) + K\left(\frac{2 - q - q_i}{h_i}\right). \quad (12)$$

Although use of reflective boundary conditions ensures that \hat{f} remains within bounds, it imposes the possibly unphysical constraint that $d\hat{f}/dq = 0$ at $q = 0$ and $q = 1$.

The estimated distributions $\hat{f}(q_{\text{am}})$ are shown in the left column of Figure 4, for the ‘de’, ‘de/ex’, ‘ex/de’, and ‘ex’ galaxies; the equivalent distributions $\hat{f}(q_{25})$ for the isophotal shapes are shown in the right column. In each panel of Figure 4, the heavier line indicates the shape distribution for the bright galaxies, and the lighter line indicates the distribution for the fainter galaxies. The dotted lines indicate the 98% error intervals found by bootstrap resampling. In our bootstrap analysis, we randomly selected N data points, with substitution, from the original sample of N axis ratios. We then created a new estimate \hat{f} from the bootstrapped data. After doing 1000 bootstrap estimates, we then determined the 98% error intervals: in Figure 4, 1% of the bootstrap estimates lie above the upper dotted line, and 1% of the bootstrap estimates lie below the lower dotted line.

Note from the upper left panel of Figure 4 that the bright ‘de’ galaxies have a distribution that peaks at $q_{\text{am}} \approx 0.84$, similar to the result found for relatively bright elliptical galaxies (Benacchio & Galletta 1980; Fasano & Vio 1991; Franx, Illingworth, & de Zeeuw 1991; Lambas, Maddox, & Loveday 1992). The faint ‘de’ galaxies have a flatter modal shape ($q_{\text{am}} \approx 0.70$) and a broader distribution of shapes. Both the bright and faint ‘de’ galaxies have a relative scarcity of galaxies with $q_{\text{am}} = 1$; this is the usual sign that the galaxies in the population cannot be purely oblate. For ‘de’ galaxies, the difference between the adaptive moments shapes and the isophotal shapes is intriguing. Note that $\hat{f}(q_{25})$ for the ‘de’ galaxies, shown in the upper right panel of Figure 4, peaks at $q_{25} \approx 0.76$ for the bright galaxies. For the fainter ‘de’ galaxies, the distribution of isophotal axis ratios, though it peaks at $q_{25} \approx 0.74$, is very broad. An axis ratio distribution \hat{f} that is nearly constant over a broad range of q is the signature of a population of flattened disks. The distribution $\hat{f}(q_{25})$ drops at $q \lesssim 0.2$, indicating that the disks are not infinitesimally thin, and at $q \gtrsim 0.9$, indicating that the disks are not perfectly circular.

The distribution of shapes for ‘de/ex’ galaxies are seen in the second row of Figure 4. As with all profile types, the bright galaxies are rounder on average than the fainter galaxies. Both bright and faint ‘de/ex’ galaxies have a scarcity of nearly circular galaxies. Particularly noteworthy is the distinct difference between $\hat{f}(q_{\text{am}})$ for the bright ‘de’ galaxies, very strongly peaked at $q_{\text{am}} \approx 0.84$, and the equivalent distribution $\hat{f}(q_{\text{am}})$ for the bright ‘de/ex’ galaxies, which is much broader and peaks at the flatter shape of $q_{\text{am}} \approx 0.67$.

The ‘ex/de’ and ‘ex’ galaxies in our sample have, by definition, $\text{fracDeV} < 0.5$ and hence Sérsic index $n \lesssim 2$. We expect these galaxies to be predominantly disk-dominated spiral galaxies. Determining the true distribution of intrinsic axis ratios for spiral galaxies is complicated by the presence of dust. A magnitude-limited sample of dusty spiral galaxies will show a deficit of galaxies with high inclination and low apparent axis ratio. This deficit is due to internal extinction by dust; in the B band, for instance, a spiral galaxy of type Sc will be up to 1.5 mag fainter when seen edge-on than when seen face-on (Huizinga & van Albada 1992). In the r band, the inclination-dependent dimming is not as great, but will still affect the observed distribution of axis ratios in a magnitude-limited sample such as the SDSS spectroscopic galaxy sample (Ryden 2004). A dusty disk galaxy which would qualify as a bright ‘ex’ galaxy if seen face-on might only qualify as a faint ‘ex’ galaxy when seen edge-on. Similarly, a less luminous galaxy, which would qualify only as a faint ‘ex’ galaxy when seen face-on, might drop out of our sample entirely when seen edge-on. The main effect of dust on the distribution of q for a magnitude-limited survey of spiral galaxies is to reduce the number of galaxies with $q \lesssim 0.5$; the distribution for $q \gtrsim 0.5$ is not strongly affected (Huizinga & van Albada 1992).

With the caveat that we are undercounting edge-on, low- q galaxies, the observed axis ratios for ‘ex/de’ and ‘ex’ galaxies are shown in the bottom two rows of Figure 4. The shapes of ‘ex/de’ galaxies, as measured by either q_{am} or q_{25} , spread over a wide range of axis ratios, with bright ‘ex/de’ galaxies being slightly rounder, on average, than the fainter galaxies. The shapes of ‘ex’ galaxies are very similar to the shapes of ‘ex/de’ galaxies. For the ‘ex/de’ and ‘ex’ galaxies, the dip in \hat{f} at $q \gtrsim 0.9$ is a consequence of the fact that the disks of these galaxies are not perfectly circular.

4. INTRINSIC SHAPES

Having a smooth kernel estimate \hat{f} for the distribution of apparent axis ratios q permits us to estimate the distribution of intrinsic axis ratios γ , given the assumption that all galaxies have the same value of the triaxiality parameter T . We don’t necessarily expect all the galaxies of a given profile type to have the same triaxiality; cosmological simulations, as well as simulations of merging galaxies, generally give a range of T (see Statler et al. (2004) and references therein) for bright galaxies. However, by assuming uniform triaxiality and seeing which values of T yield physically plausible results, we can get a feel for which values of T are data-friendly, and which are incompatible with the data. Let $\hat{N}_T(\gamma)$ be the estimated distribution of intrinsic axis ratios, given an assumed value for T . The relation between $\hat{f}(q)$

and $\hat{N}_T(\gamma)$ is (Binney 1985):

$$\hat{f}(q) = \int_0^q P_T(q|\gamma)N_T(\gamma)d\gamma , \quad (13)$$

where $P_T(q|\gamma)dq$ is the probability that a galaxy with intrinsic short-to-long axis ratio γ and triaxiality T has an apparent axis ratio in the range $q \rightarrow q + dq$, when viewed from a random orientation.

Equation (13) represents a Volterra equation of the first kind which can be solved by standard numerical techniques. We first compute \hat{f} on 200 points equally spaced in q , using the kernel technique previously described. We then compute P_T on an 200×200 grid in (q, γ) space. For each value of γ , we compute an adaptive kernel estimate for P_T by randomly choosing a large number of viewing angles ($\sim 10^5$), then computing what the apparent axis ratio q would be for each viewing angle, given the assumed values of γ and T (Binney 1985). The kernel estimate of the distribution of q is then our estimate of $P_T(q|\gamma)$. Equation (13), in its discretized form, can be written

$$\hat{f}_k = \sum_{j=1}^k P_{T,kj} \hat{N}_{T,j} . \quad (14)$$

Since $P_{T,kj} = 0$ for $j > k$ (the apparent axis ratio of a galaxy can't be less than its intrinsic axis ratio), the matrix \mathbf{P}_T is lower triangular, and equation (14) can be inverted simply by forward substitution (Press et al. 1992).

We performed the inversion to find \hat{N}_T using six different values of the triaxiality: $T = 0$ (oblate), $T = 0.2$, $T = 0.4$, $T = 0.6$, $T = 0.8$, and $T = 1$ (prolate). When our ultimate goal is finding \hat{N}_T , determining the optimal kernel width h for \hat{f} is a vexed question. It is generally true that the best value of h for estimating \hat{N}_T is greater than the best value of h for purpose of estimating \hat{f} (Tremblay & Merritt 1995, 1996); N_T is a deconvolution of f , and the deconvolution process increases the noise present. Tremblay & Merritt (1995) proposed, for the purposes of estimating N_T , using the value of h that minimized

$$\text{BMISE}(h) = \int_0^1 [\hat{N}_T(\gamma) - \hat{N}_T^*(\gamma)]^2 d\gamma , \quad (15)$$

where \hat{N}_T^* is an estimate of N_T from a bootstrap resampling of the original data. Unfortunately, we found, as Tremblay & Merritt (1995) did, that $\text{BMISE}(h)$ returns badly oversmoothed estimates of N_T . Thus, we fell back on using our subjective impressions of the smoothness of \hat{N}_T , and ended by taking the value of h given by equation (10) and multiplying by a factor of 1.5.

To perform the inversion and find the estimated distribution of γ , we assumed that all galaxies have the same triaxiality T . If this assumption is incorrect, then the inversion of equation (14) may result in $\hat{N}_T < 0$ for some range of γ , which is physically impossible. To exclude our hypothesis (that all galaxies have triaxiality T) at some fixed statistical confidence level, we can repeat the inversion for a large number of bootstrap resamplings of the original data set. In practice, we did 1000 resamplings, and used them to place 98% confidence intervals on \hat{N}_T . If the confidence interval falls below zero for some value of γ , then the hypothesized value of T can be rejected at the 99% (one-sided) confidence level.

Figure 5 shows the distribution of intrinsic shapes for ‘de’ galaxies ($\text{fracDeV} > 0.9$), when the adaptive moments axis ratio q_{am} is used as the estimator of the apparent shape. The heavy line is the distribution for the bright ‘de’ galaxies ($M_r \leq -21.8$) and the light line is the distribution for the fainter ‘de’ galaxies. The assumed value of T is shown in each panel, ranging from purely oblate shapes, with $T = 0$, in the upper left corner to purely prolate shapes, with $T = 1$, in the lower right corner.

An eye-catching feature of Figure 5 is the oscillatory nature of \hat{N}_T in the triaxial cases. The multiple peaks in \hat{N}_T at high γ result from the shape of the conditional probability function $P_T(q|\gamma)$ for highly triaxial galaxies. When galaxies are axisymmetric ($T = 0$ or 1), the conditional probability peaks at $q = \gamma$, the minimum possible apparent axis ratio. For triaxial galaxies, however, the conditional probability has one or more local maxima at $q > \gamma$. To see why this can result in oscillatory solutions consider \hat{N}_T for faint ‘de’ galaxies when $T = 0.8$; this is shown by the light line in the lower left panel of Figure 5. The distribution \hat{N}_T has a local maximum at $\gamma = 0.42$. For $T = 0.8$, the conditional probability $P_T(q|\gamma = 0.42)$ peaks at $q = 0.57$. Thus, the large number of $\gamma \approx 0.42$ galaxies result in many galaxies with an apparent axis ratio $q \approx 0.57$; so many, in fact, that \hat{N}_T must be made very small in the range $0.42 < \gamma < 0.57$ in order to avoid overproducing $q \approx 0.57$ galaxies. In fact, as seen in Figure 5, \hat{N}_T has a local minimum at $\gamma = 0.54$, at which \hat{N}_T falls slightly below zero. Since $P_T(q|\gamma = 0.54)$ peaks at $q = 0.65$, this produces a deficit of $q \approx 0.65$ galaxies, which must be compensated for by making \hat{N}_T very large in the range $0.54 < \gamma < 0.65$. In fact, \hat{N}_T has another local maximum at $q = 0.62$. And so the oscillations continue, with decreasing wavelength, until $\gamma = 1$ is reached. Tremblay & Merritt (1995) found that $\hat{N}(\gamma)$ for bright elliptical galaxies was significantly bimodal if the galaxies were assumed to be highly triaxial; this bimodality also had its origin in the shape of the conditional probability function for triaxial galaxies.

For both bright and faint ‘de’ galaxies, using q_{am} as the apparent axis ratio, oblate fits are statistically unacceptable, producing a negative number of galaxies with $\gamma \gtrsim 0.9$ (see the upper left panel of Figure 5). For bright ‘de’ galaxies, statistically acceptable fits are found

for $T = 0.4, 0.6,$ and 0.8 ; that is, their 98% confidence intervals never fall entirely below zero. The mean intrinsic axis ratio for the acceptable fits ranges from $\langle\gamma\rangle = 0.66$ for $T = 0.4$ to $\langle\gamma\rangle = 0.69$ for $T = 0.8$. The permissible fits for the bright ‘de’ galaxies are consistent with the deduced triaxial shape of the nearby bright ($M_r \sim -22.2$) elliptical galaxy NGC 4365, for which a combination of photometric and kinematic data yields $T \sim 0.45$ and $\gamma \sim 0.6$ (Statler et al. 2004). Although the bright ‘de’ galaxies are best fit by highly triaxial shapes, the faint ‘de’ galaxies are best fit by nearly prolate shapes, with $T = 0.8$ and $T = 1$ both giving statistically acceptable fits. (The highly oscillatory solution for $T = 0.8$ may be physically dubious – why should galaxy shapes be quantized? – but it is statistically acceptable.) The mean intrinsic shape of faint ‘de’ galaxies is $\langle\gamma\rangle = 0.53$ if $T = 0.8$ and $\langle\gamma\rangle = 0.58$ if $T = 1$.

Figure 6 shows the deduced distribution of intrinsic shapes for ‘de’ galaxies when the isophotal axis ratio q_{25} is used, rather than the adaptive moments axis ratio. The bright ‘de’ galaxies have a statistically acceptable fit when $T = 0.4, T = 0.6, T = 0.8,$ and $T = 1$. The mean intrinsic shape ranges from $\langle\gamma\rangle = 0.51$ when $T = 0.4$ to $\langle\gamma\rangle = 0.62$ when $T = 1$. The fainter ‘de’ galaxies are acceptably fit, assuming constant triaxiality, only when $T = 1$, which results in $\langle\gamma\rangle = 0.51$. The $T = 0$ case, which can be rejected at the 99% confidence level but not at the 99.9% level, would produce $\langle\gamma\rangle = 0.28$; this axis ratio is flatter than that of an ice hockey puck. (Although the $T = 0$ and $T = 0.2$ fits are statistically unacceptable at the 99% confidence level, the data are consistent with a population of nearly oblate shapes if we relax the assumption of uniform T . For instance, the faint ‘de’ galaxies can be fit at the 99% confidence level, with a Gaussian distribution of T peaking at $T = 0$ and with $\sigma_T = 0.2$.)

The shapes of ‘de/ex’ galaxies can be analyzed in the same way as the shapes of ‘de’ galaxies. For instance, the distributions of intrinsic shapes for ‘de/ex’ galaxies, using q_{am} as the apparent axis ratio, are shown in Figure 7. For the brighter galaxies with ‘de/ex’ profiles, acceptable fits are found when $T = 0.8$, yielding $\langle\gamma\rangle = 0.51$, and when $T = 1$, yielding $\langle\gamma\rangle = 0.57$. For the fainter ‘de/ex’ galaxies, only the $T = 1$ fit is statistically acceptable, yielding a mean intrinsic axis ratio of $\langle\gamma\rangle = 0.48$ for the prolate galaxies. Notice that bright ‘de/ex’ galaxies, faint ‘de/ex’ galaxies, and faint ‘de’ galaxies all are consistent with having shapes, at least in their inner regions, which are prolate, or nearly prolate, with a typical axis ratio of $\langle\gamma\rangle \sim 1/2$. Bright ‘de’ galaxies are distinctly different, with shapes that are consistent with their being highly triaxial, with a typical axis ratio of $\langle\gamma\rangle \sim 2/3$.

The intrinsic shape distributions for ‘de/ex’ galaxies, using q_{25} as the apparent shape measure, are shown in Figure 8. For both the bright and faint ‘de/ex’ galaxies, the $T = 1$ fit is statistically acceptable. For the prolate fits, the average shape of the bright ‘de/ex’ galaxies is $\langle\gamma\rangle = 0.55$, and the average shape of the faint ‘de/ex’ galaxies is $\langle\gamma\rangle = 0.47$. Thus, given the prolate hypothesis, ‘de/ex’ galaxies are only slightly flatter in their outer regions,

whose shape is measured by q_{25} , than in their inner regions, whose shape is measured by q_{am} .

With the repeated caveat that we are undercounting edge-on, low- q galaxies, the results for the ‘ex/de’ galaxies are presented in Figures 9 and 10. When q_{am} is used as the measure of apparent shape (Figure 9), the bright ‘ex/de’ galaxies have a statistically acceptable fit when $T = 0.8$, which results in $\langle\gamma\rangle = 0.49$; the $T = 1$ fit, which goes slightly negative at $\gamma \gtrsim 0.94$, yields a mean intrinsic axis ratio of $\langle\gamma\rangle = 0.55$. None of the six tested triaxialities gave an acceptable fit, at the 99% confidence level, to the faint ‘ex/de’ galaxies. The best (or the ‘least bad’) of the fits, with $T = 1$, yields $\langle\gamma\rangle = 0.49$. When q_{25} is used as the measure of apparent shape (Figure 10), none of the tested values of T gives a fit acceptable at the 99% confidence level. The best fit, for both bright and faint galaxies, is given by $T = 1$, for which $\langle\gamma\rangle = 0.55$ for the bright ‘ex/de’ galaxies and $\langle\gamma\rangle = 0.50$ for the faint ‘ex/de’ galaxies.

As with the ‘ex/de’ galaxies, the sample of ‘ex’ galaxies is affected by an undercount of low- q galaxies. With this caveat, the results for the ‘ex’ galaxies are shown in Figures 11 and 12. In general, the results are similar to those for ‘ex/de’ galaxies. When the axis ratios of ‘ex’ galaxies are estimated using q_{am} (Figure 11), the bright ‘ex’ galaxies are acceptably fit when $T = 0.8$, yielding $\langle\gamma\rangle = 0.49$; the $T = 1$ fit for the bright ‘ex’ galaxies, which goes slightly negative at high γ , yields $\langle\gamma\rangle = 0.56$. The best fit to the faint ‘ex’ galaxies is provided by the $T = 1$ inversion, which yields $\langle\gamma\rangle = 0.46$. When q_{25} is used as the estimate of the apparent axis ratio (Figure 12), the results are extremely similar. For bright ‘ex’ galaxies, only $T = 0.8$, of the tested triaxialities, gave a fit acceptable at the 99% confidence level, yielding $\langle\gamma\rangle = 0.51$; the not-as-good $T = 1$ fit gave $\langle\gamma\rangle = 0.57$. The best fit for faint ‘ex’ galaxies had $T = 1$, $\langle\gamma\rangle = 0.49$.

Although the best fits to the ‘ex/de’ and ‘ex’ galaxies, under the assumption of constant triaxiality, were prolate or nearly prolate, we have an a priori knowledge that bright galaxies with Sérsic index $n \lesssim 2$ are generally rotationally supported disks. The SDSS DR3 photometry of ‘ex/de’ and ‘ex’ galaxies is consistent with their being nearly oblate objects only if they have a range of T , instead of being forced into a straitjacket of uniform T .

5. DISCUSSION

Constraining the flattening γ and triaxiality T of galaxies with different luminosity and profile type provides potentially useful clues for the study of galaxy formation and evolution. For example, the dissipationless merger of two equal-mass disk galaxies embedded within dark halos produces a merger remnant whose luminous component has an approximate de

Vaucouleurs profile (Barnes 1992). The values of γ and T of the remnant depend on the initial orbital parameters of the merging galaxies, but the remnant is typically quite flat and prolate. For a set of eight simulations with different initial orbits, Barnes (1992) found $\langle\gamma\rangle \sim 0.5$ and $\langle T\rangle \sim 0.7$ for the most tightly bound quartile of the luminous particles (the inner region of the galaxy). This is significantly flatter and more prolate than the shape we deduced from the distribution of q_{am} for bright ‘de’ galaxies. The oblateness of the merger remnant is increased, however, if the initial merging galaxies are unequal in mass (Barnes 1998; Naab & Burkert 2003).

Including gaseous dissipation into a simulated merger can strongly affect γ and T . As the gas dissipates and falls toward the center of the merger remnant, the central mass concentration will scatter stars on low angular momentum box orbits, thus acting to increase γ and decrease T . For instance, a simulated remnant that has $\gamma \approx 0.55$ and $T \approx 0.8$ in the absence of dissipation will have $\gamma \approx 0.65$ and $T \approx 0.5$ if gas dissipation is added (Barnes 1998). The deduced shapes of bright ‘de’ galaxies are consistent with their being merger remnants, as long as the mergers were dissipational.

In the standard hierarchical clustering model for structure formation, however, we do not expect most elliptical galaxies to have formed by the relatively recent merger of a pair of spiral galaxies. More typically, an elliptical galaxy will have formed by the successive merger of a number of smaller galaxies or subgalactic “clumps”. Simulations of multiple mergers in small groups reveal that the final merger remnant generally has a surface brightness profile similar to a de Vaucouleurs law, but that the shape of the merger remnant depends on the assumed initial conditions (Weil & Hernquist 1996; Garijo, Athanassoula, & García-Gómez 1997; Zhang et al. 2002). For instance, Zhang et al. (2002) simulated dissipationless mergers of dense clumps embedded in a smooth dark halo. The profile of the merger remnant, in all cases, was well fit by a de Vaucouleurs law. The triaxiality of the remnant depended primarily on whether the system was initially in a state of virial equilibrium or in a state of non-virial collapse. The virial case produced more oblate remnants ($\langle T\rangle \sim 0.3$), while the collapse case produced more prolate remnants ($\langle T\rangle \sim 0.7$). The virial case also produced less flattened remnants: $\langle\gamma\rangle \sim 0.8$ for the merger remnants of initially virialized systems versus $\langle\gamma\rangle \sim 0.6$ for initially collapsing systems. The value of γ also depended on the initial clump-to-halo mass ratio; if the clumps contributed only a small fraction of the total mass, they produced a flatter remnant than if they contributed all the mass, with no dark halo. The best fitting parameters for the bright ‘de’ galaxies, $\mu_\gamma = 0.66$ and $T_0 = 0.43$, suggest that they are too flattened and too triaxial to have been formed primarily by mergers within a virialized group, which produce $\langle\gamma\rangle \sim 0.8$ and $\langle T\rangle \sim 0.3$. (Remember, the effects of dissipation will only act to increase γ and decrease T .)

Another influence that is capable of increasing γ and decreasing T is the presence of a central supermassive black hole. A central mass concentration affects the structure of the surrounding galaxy by disrupting box orbits (Gerhard & Binney 1985; Norman, May, & van Albada 1985). The resulting chaotic orbits lead to an altered shape for the galaxy; the trend is toward shapes that are nearly spherical in the inner regions and nearly oblate in the outer regions (Merritt & Quinlan 1998). In the inner regions, the orbits can support a shape that is nearly oblate, $T \sim 0.25$, or strongly triaxial, $T \sim 0.5$, but not nearly prolate, $T \sim 0.75$ (Poon & Merritt 2004). The time scale for the shape evolution depends on the mass of the central black hole relative to the total stellar mass of the galaxy. When the central black hole has a mass equal to 1% of the mass in stars, its shape at the half-mass radius evolves in ~ 40 times the half-mass orbital period; when the mass is only 0.3% of the stellar mass, the evolution time scale increases to ~ 200 times the orbital period. The observed relation between central black hole mass and bulge mass (Merritt & Ferrarese 2001; Marconi & Hunt 2003; Häring & Rix 2004) predicts that an elliptical galaxy will typically have a central black hole with a mass $\lesssim 0.2\%$ of the total mass in stars. For such relatively low black hole masses, the shape evolution time scale at the half-mass radius and beyond will exceed the age of the galaxy. Thus, a central black hole will not generally affect the isophotal axis ratio q_{25} .

The isophotal shape, q_{25} , measures the apparent shape of a galaxy at a few times the effective radius. Converted to physical units, the average semimajor axis A_{25} of the isophotal ellipse ranges from $\langle A_{25} \rangle = 2.4$ kpc at $M_r = -16$ to $\langle A_{25} \rangle = 45$ kpc at $M_r = -23$. At relatively high luminosities ($M_r \lesssim -20.5$), the mean value of q_{25} increases with luminosity; bright galaxies are rounder than fainter galaxies at their outer regions. We have also uncovered the puzzling result that at a given luminosity, the mean value of q_{25} is larger for ‘ex’ galaxies than for ‘de’ galaxies. Why should ‘ex’ galaxies, which are flattened disks in their central regions, be rounder than ‘de’ galaxies in their outskirts? At such great distances from the galaxy’s center, we expect that tidal distortions from neighboring galaxies will significantly affect the isophotal shape. Galaxies in dense regions, such as the cores of clusters, are subject to more interactions with neighboring galaxies, and may well differ systematically in shape from field galaxies, which are less frequently harassed. Since elliptical galaxies are found preferentially in dense environments, this conjectured environment – shape relation would then translate into a relation between profile type and shape. A future paper, studying the relation between apparent axis ratio and environment for SDSS DR3 galaxies (Kuehn & Ryden, 2005, in preparation), will test this conjecture.

Richard Pogge, Fred Kuehn, and the anonymous referee provided useful assistance and comments.

Funding for the creation and distribution of the SDSS Archive has been provided by

the Alfred P. Sloan Foundation, the Participating Institutions, the National Aeronautics and Space Administration, the National Science Foundation, the U.S. Department of Energy, the Japanese Monbukagakusho, and the Max Planck Society. The SDSS website is <http://www.sdss.org/>. The SDSS is managed by the Astrophysical Research Consortium (ARC) for the Participating Institutions. The Participating Institutions are The University of Chicago, Fermilab, the Institute for Advanced Study, the Japan Participation Group, The Johns Hopkins University, Los Alamos National Laboratory, the Max-Planck-Institute for Astronomy (MPIA), the Max-Planck-Institute for Astrophysics (MPA), New Mexico State University, University of Pittsburgh, Princeton University, the United States Naval Observatory, and the University of Washington.

REFERENCES

- Abazajian, K., et al. 2003, *AJ*, 126, 2081
- Abazajian, K. et al. 2004, *AJ*, 128, 502
- Abazajian, K. et al. 2005, *AJ*, submitted (astro-ph/0410239)
- Abramson, I. S. 1982, *Annals of Statistics*, 10, 1217
- Alam, S. M. K., & Ryden, B. S. 2002, *ApJ*, 570, 610
- Barnes, J. E. 1992, *ApJ*, 393, 484
- Barnes, J. E. 1998, in *Galaxies: Interactions and Induced Star Formation*, ed. D. Friedli, L. Martinet, & D. Pfenniger (Saas-Fee Adv. Course 26; Berlin: Springer), 275
- Benacchio, L., & Galletta, G. 1980, *MNRAS*, 193, 885
- Bernstein, G. M., & Jarvis, M. 2002, *AJ*, 123, 583
- Binney, J. 1985, *MNRAS*, 212, 767
- Blanton, M. R., et al. 2003, *ApJ*, 594, 186
- de Vaucouleurs, G. 1948, *Ann. d’Astrophys.* 11, 247
- de Vaucouleurs, G. 1959, *Handb. Phys.* 53, 275
- Fall, M., & Frenk, C. S. 1983, *AJ*, 88, 1626
- Fasano, G., & Vio, R. 1991, *MNRAS*, 249, 629

- Franx, M., Illingworth, G., & de Zeeuw, T. 1991, *ApJ*, 383, 112
- Freeman, K. C. 1970, *ApJ*, 160, 811
- Fukugita, M., Shimasaku, K., Ichikawa, T. 1995, *PASP*, 107, 945
- Fukugita, M., Ichikawa, T., Gunn, J. E., Doi, M., Shimasaku, K., & Schneider, D. P. 1996, *AJ*, 111, 1748
- Garijo, A., Athanassoula, E., & García-Gómez, C. 1997, *A&A*, 327, 930
- Gerhard, O. E., & Binney, J. 1985, *MNRAS*, 216, 467
- Gunn, J. E., et al. 1998, *AJ*, 116, 3040
- Håring, N., & Rix, H.-W. 2004, *ApJ*, 604, L89
- Hirata, C., & Seljak, U. 2003, *MNRAS*, 343, 459
- Hubble, E. 1926, *ApJ*, 64, 321
- Huizinga, J. E., & van Albada, T. S. 1992, *MNRAS*, 254, 677
- Lambas, D. G., Maddox, S., & Loveday J. 1992, *MNRAS*, 258, 404
- Marconi, A., & Hunt, L. K. 2003, *ApJ*, 589, L21
- Merritt, D., & Ferrarese, L. 2001, *MNRAS*, 320, L30
- Merritt, D., & Quinlan, G. D. 1998, *ApJ*, 498, 625
- Naab, T., & Burkert, A. 2003, *ApJ*, 597, 893
- Nakamura, O., Fukugita, M., Yasuda, N., Loveday, J., Brinkmann, J., Schneider, D. P., Shimasaku, K., SubbaRao, M. 2003, *AJ*, 125, 1682
- Norman, C. A., May, A., & van Albada, T. S. 1985, *ApJ*, 296, 20
- Poon, M. Y., & Merritt, D. 2004, *ApJ*, 606, 774
- Press, W. H., Teukolsky, S. A., Vetterling, W. T., & Flannery, B. P. 1992, *Numerical Recipes: The Art of Scientific Computing*, Second Edition (Cambridge: Cambridge University Press), ch. 2
- Roberts, M. S., & Haynes, M. P. 1994, *ARA&A*, 32, 115

- Ryden, B. S. 1992, *ApJ*, 396, 445
- Ryden, B. S. 1996, *ApJ*, 461, 146
- Ryden, B. S. 2004, *ApJ*, 601, 214
- Ryden, B. S., Forbes, D. A., & Terlevich, A. I. 2001, *MNRAS*, 326, 1141
- Sandage, A., Freeman, K. C., & Stokes, N R. 1970, *ApJ*, 160, 831
- Sérsic, J. L. 1968, *Atlas de Galaxias Australes* (Cordoba: Obs. Astron.)
- Silverman, B. W. 1986, *Density Estimation for Statistics and Data Analysis* (New York: Chapman & Hall)
- Smith, J. A., et al. 2002, *AJ*, 123, 2121
- Statler, T. S. 1994, *ApJ*, 425, 458
- Statler, T. S., Emsellem, E., Peletier, R. F., & Bacon, R. 2004, *MNRAS*, 353, 1
- Stoughton, C., et al. 2002, *AJ*, 123, 485
- Tremblay, B., & Merritt, D. 1995, *AJ*, 110, 1039
- Tremblay, B., & Merritt, D. 1996, *AJ*, 111, 2243
- Weil, M. L., & Hernquist, L. 1996, *ApJ*, 460, 101
- Vio, R., Fasano, G., Lazzarin, M., & Lessi, O. 1994, *A&A*, 289, 640
- York, D. G. et al. 2000, *AJ*, 120, 1579
- Zhang, B., Wyse, R. F. G., Stiavelli, M., & Silk, J. 2002, *MNRAS*, 332, 647

Table 1. Dividing Line Between Bright and Faint Galaxies

Profile Type	M_0	$N(M_r \leq M_0)$	$N(M_r > M_0)$	$\log P_{KS}$
de	-21.84	926	1311	-52.9
de/ex	-21.35	5235	8545	-109.2
ex/de	-21.00	11340	25305	-118.6
ex	-20.48	17101	27188	-301.9

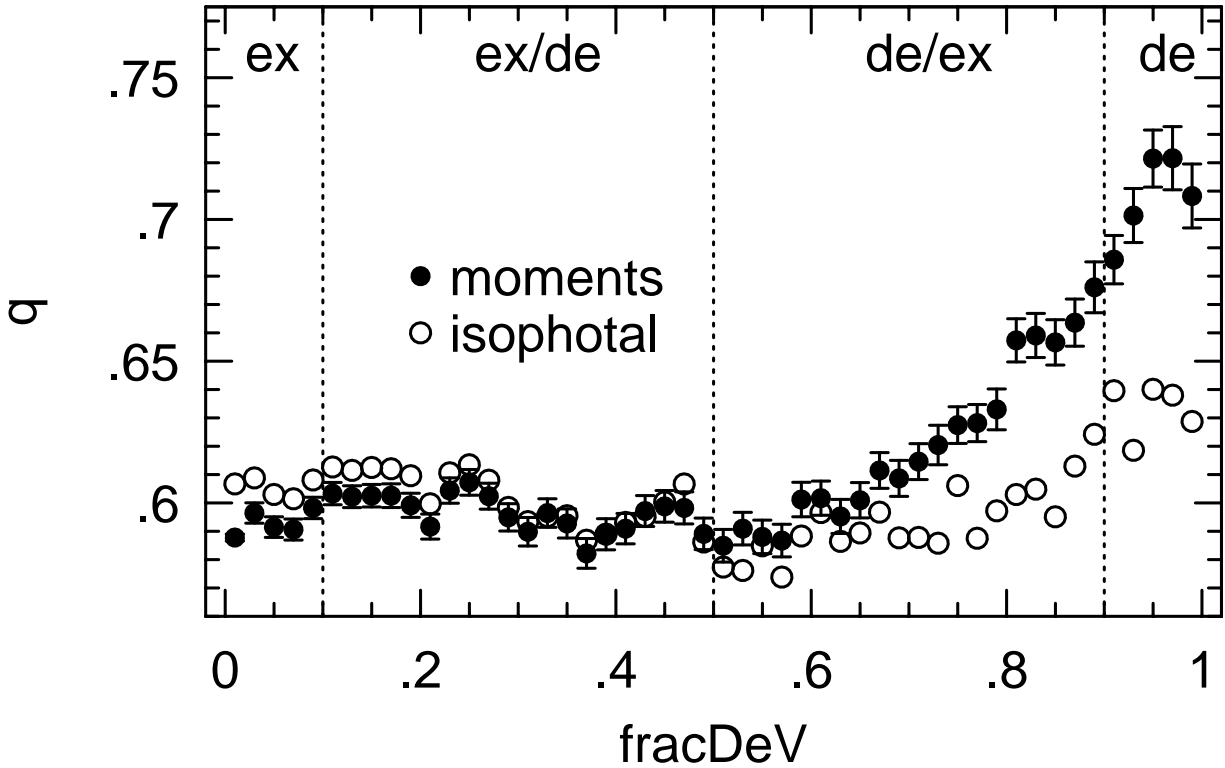


Fig. 1.— Mean apparent axis ratio $\langle q \rangle$ as a function of the SDSS fitting parameter `fracDeV`. Filled circles indicate the axis ratio estimated using the adaptive moments technique; open circles indicate the axis ratio of the 25 mag/arcsec² isophote. The error bars on the filled circles indicate the estimated error of the mean; the error bars on the open circles (not shown for clarity) are of similar size.

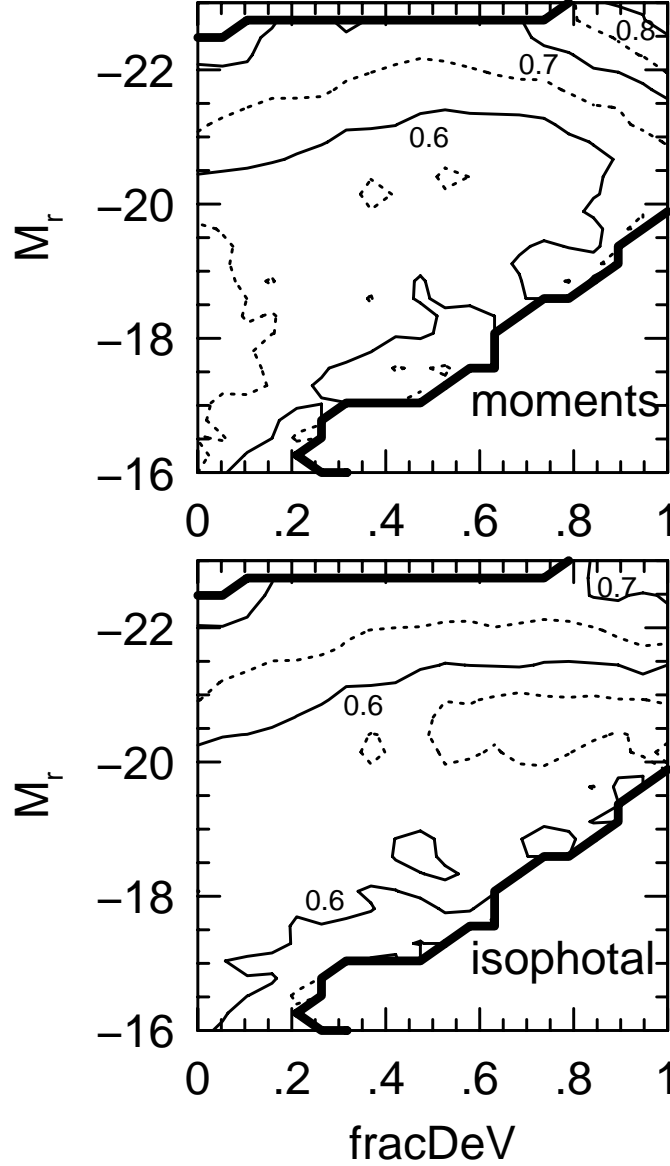


Fig. 2.— *Upper panel:* Mean apparent axis ratio q_{am} , estimated using adaptive moments, as a function of absolute magnitude M_r and fitting parameter fracDeV . Averages were computed in bins of width 0.25 mag in M_r and 0.05 in fracDeV ; the heavy line excludes the region with fewer than 25 galaxies per bin. Contours are drawn at $q = 0.6, 0.7, 0.8$ (solid lines) and at $q = 0.55, 0.65, 0.75$ (dotted lines). *Lower panel:* Same as the upper panel, using the isophotal axis ratio q_{25} as the shape estimate.

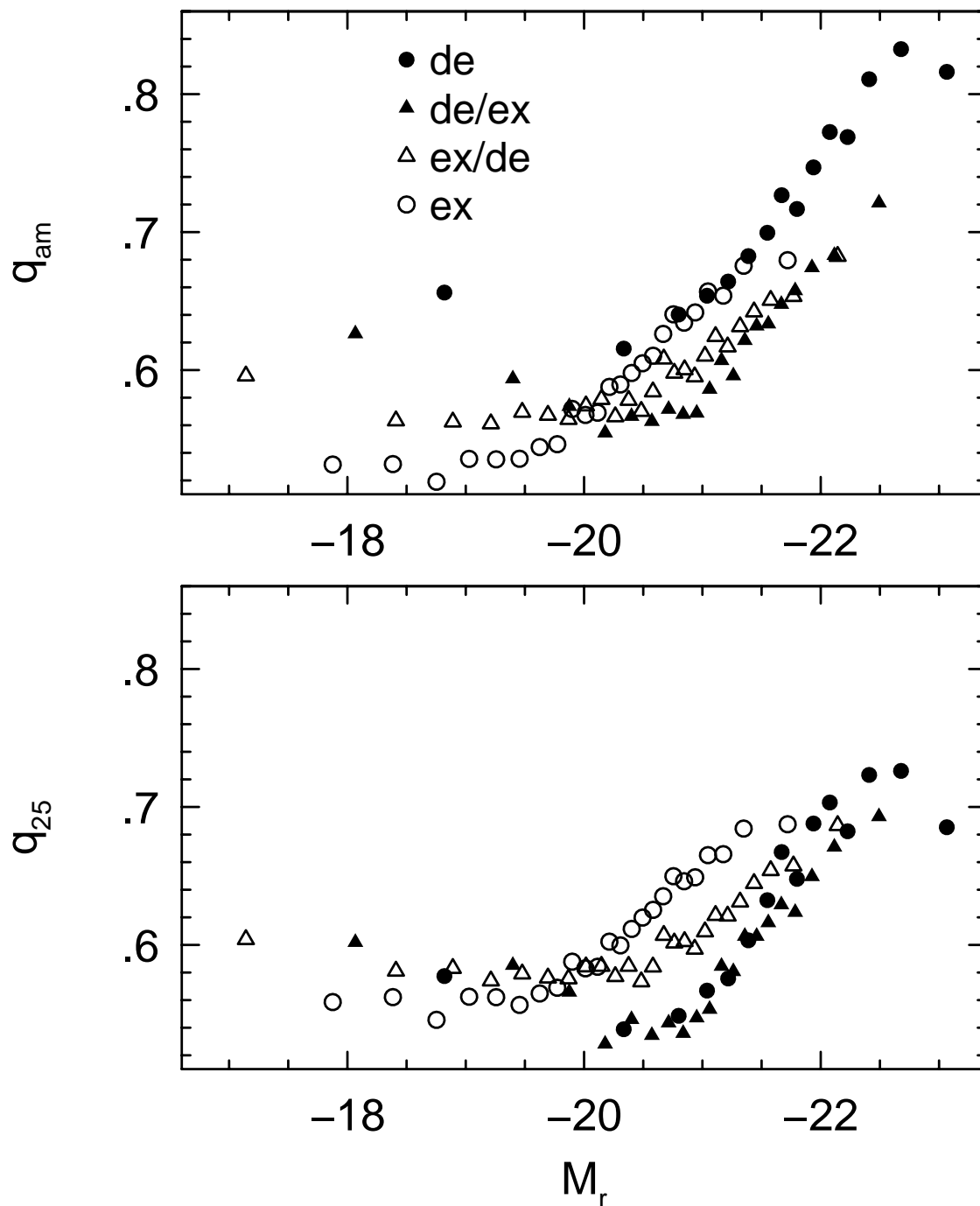


Fig. 3.— *Upper panel:* Mean apparent axis ratio q_{am} , estimated using the adaptive moments technique, as a function of absolute magnitude. The four different galaxy profile types (de, de/ex, ex/de, ex) are described in the text. *Lower panel:* Same as the upper panel, using the apparent axis ratio q_{25} of the 25 mag/arcsec² isophote.

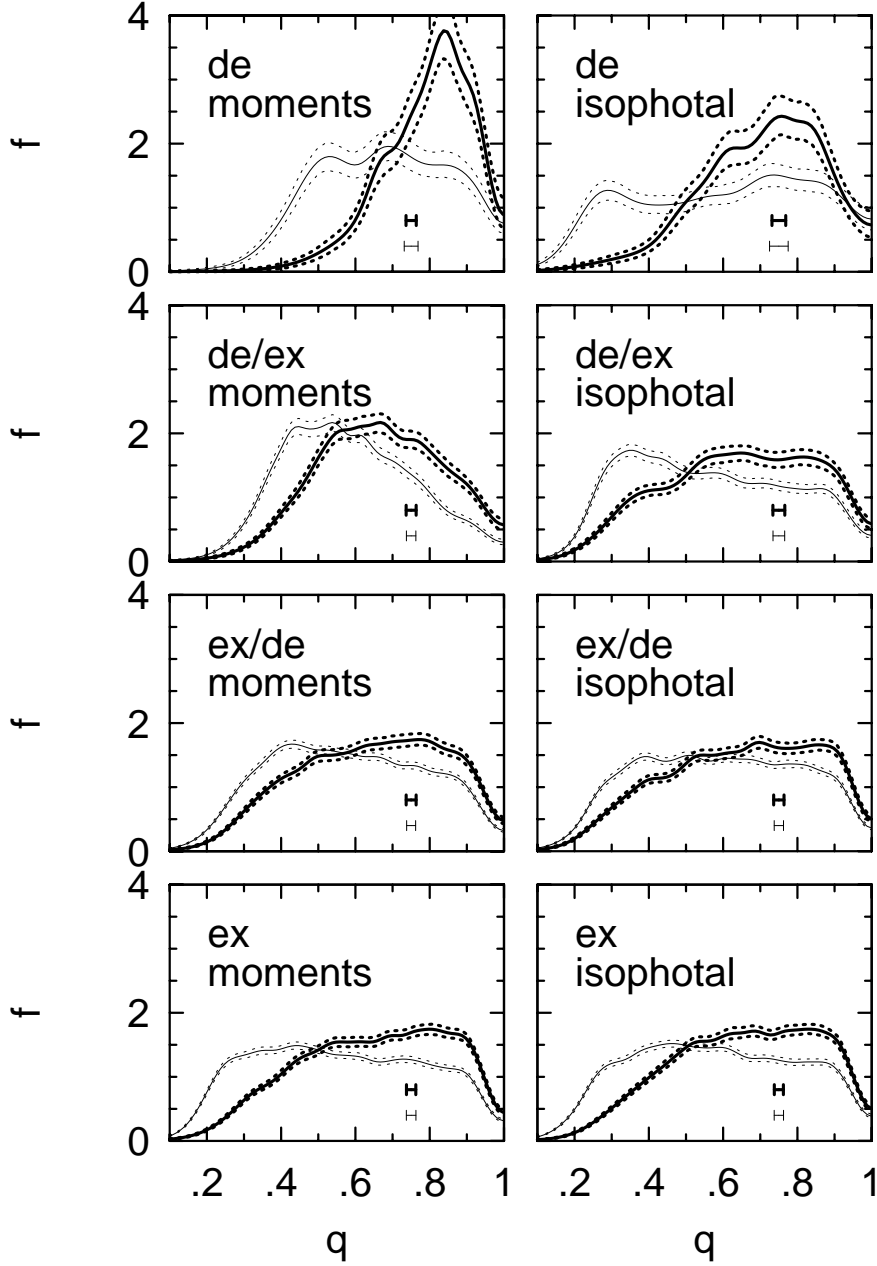


Fig. 4.— *Left column:* Distribution of the adaptive moments axis ratio q_{amb} . From top to bottom, the results are shown for profile types ‘de’, ‘de/ex’, ‘ex/de’, and ‘ex’. In each panel, the heavy line is the distribution for bright galaxies, and the light line is the distribution for faint galaxies. The dotted lines indicate the 98% confidence interval found by bootstrap resampling. The horizontal error bars indicate the kernel width h . *Right column:* The same as the left column, but using the 25 mag/arcsec² isophotal axis ratio, q_{25} , as the shape estimator.

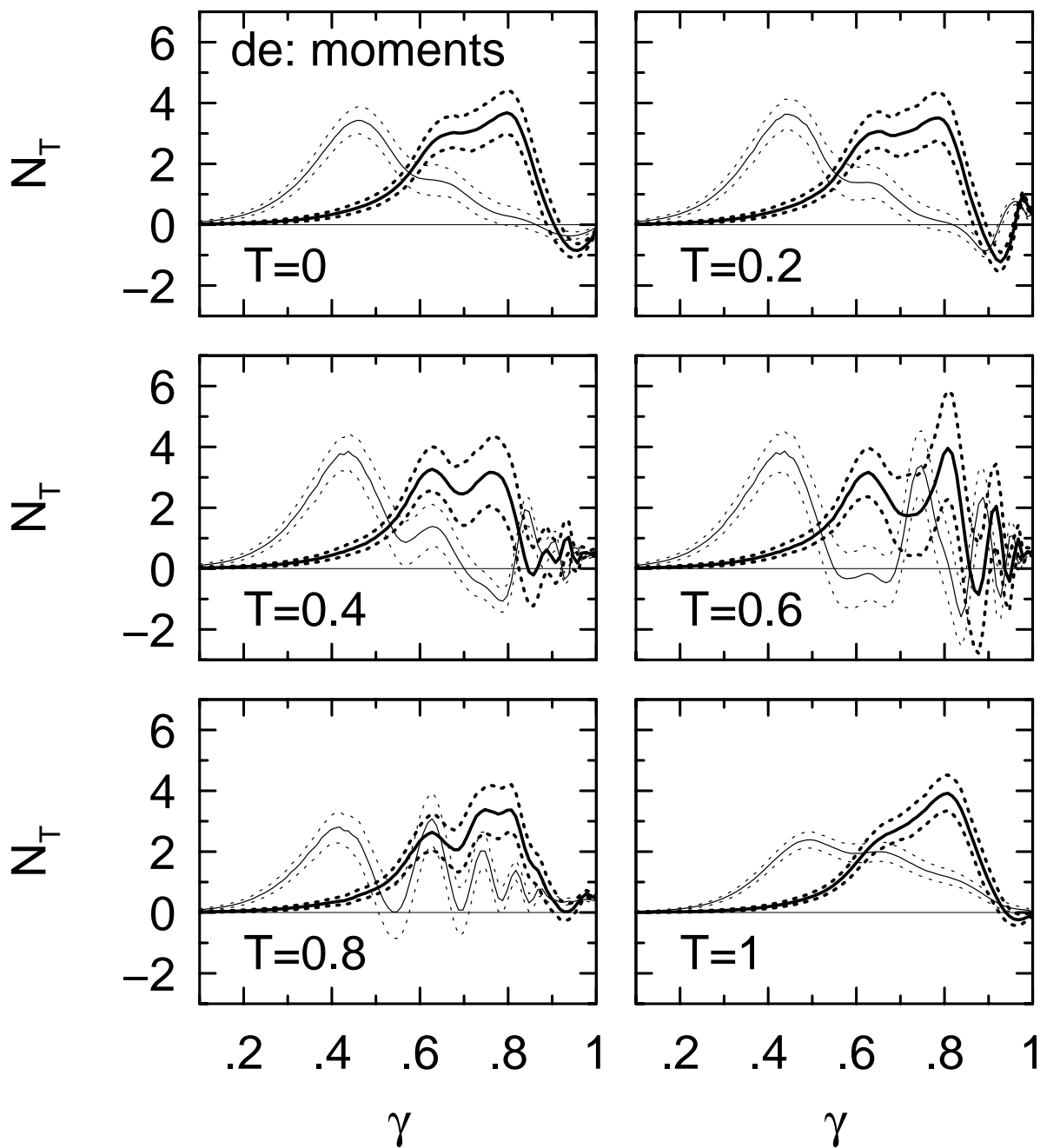


Fig. 5.— Distribution of intrinsic axis ratios for galaxies of profile type ‘de’ ($\text{fracDeV} > 0.9$), using the adaptive moments estimate of q . The heavy line is the distribution for galaxies with $M_r \leq -21.8$; the light line is for galaxies with $M_r > -21.8$. The dotted lines indicate the 98% confidence intervals, estimated by bootstrap resampling. The assumed value of the triaxiality T is given in each panel.

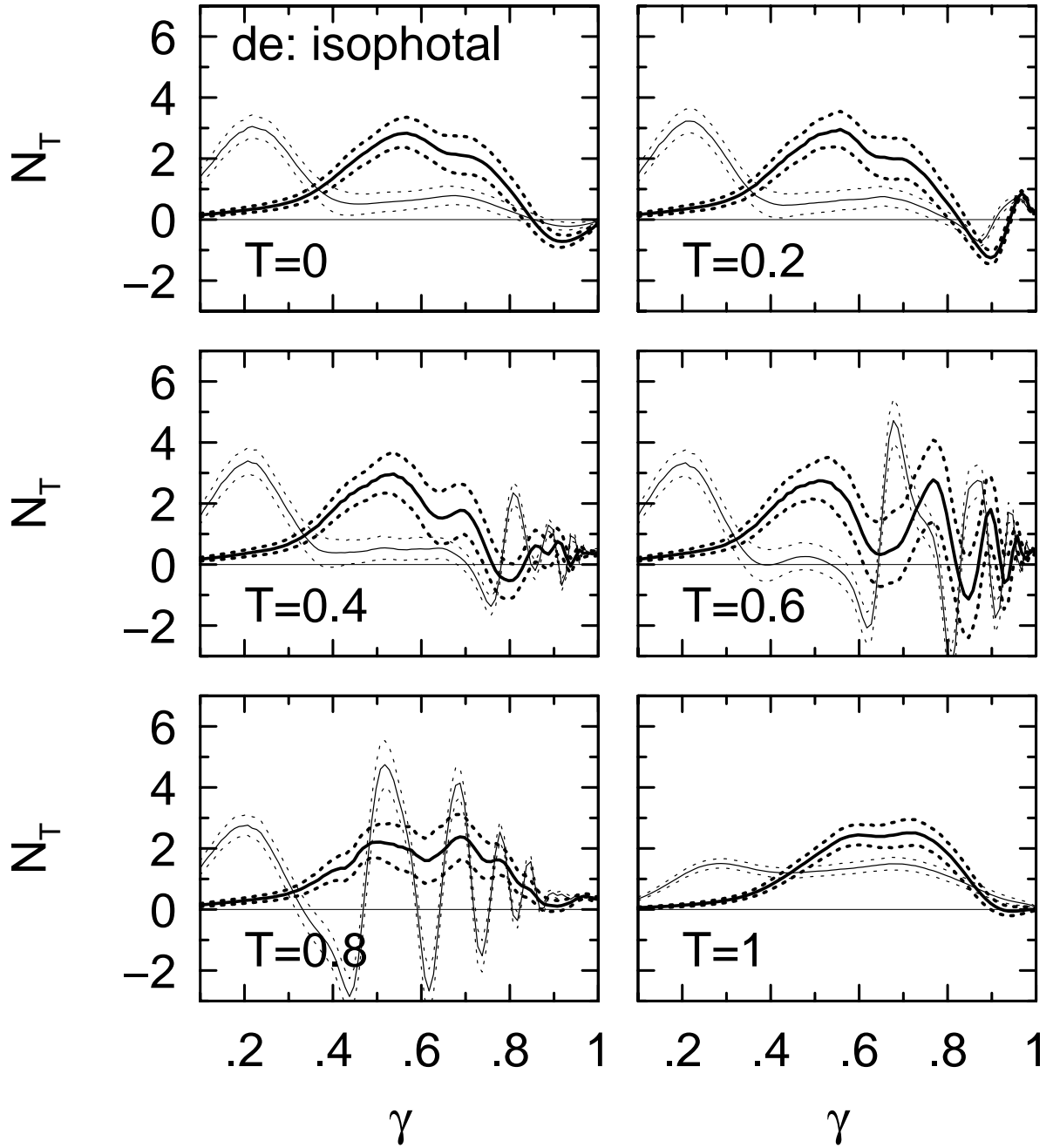


Fig. 6.— Same as Figure 5, but using the apparent axis ratio of the 25 mag/arcsec² isophote as the shape estimate.

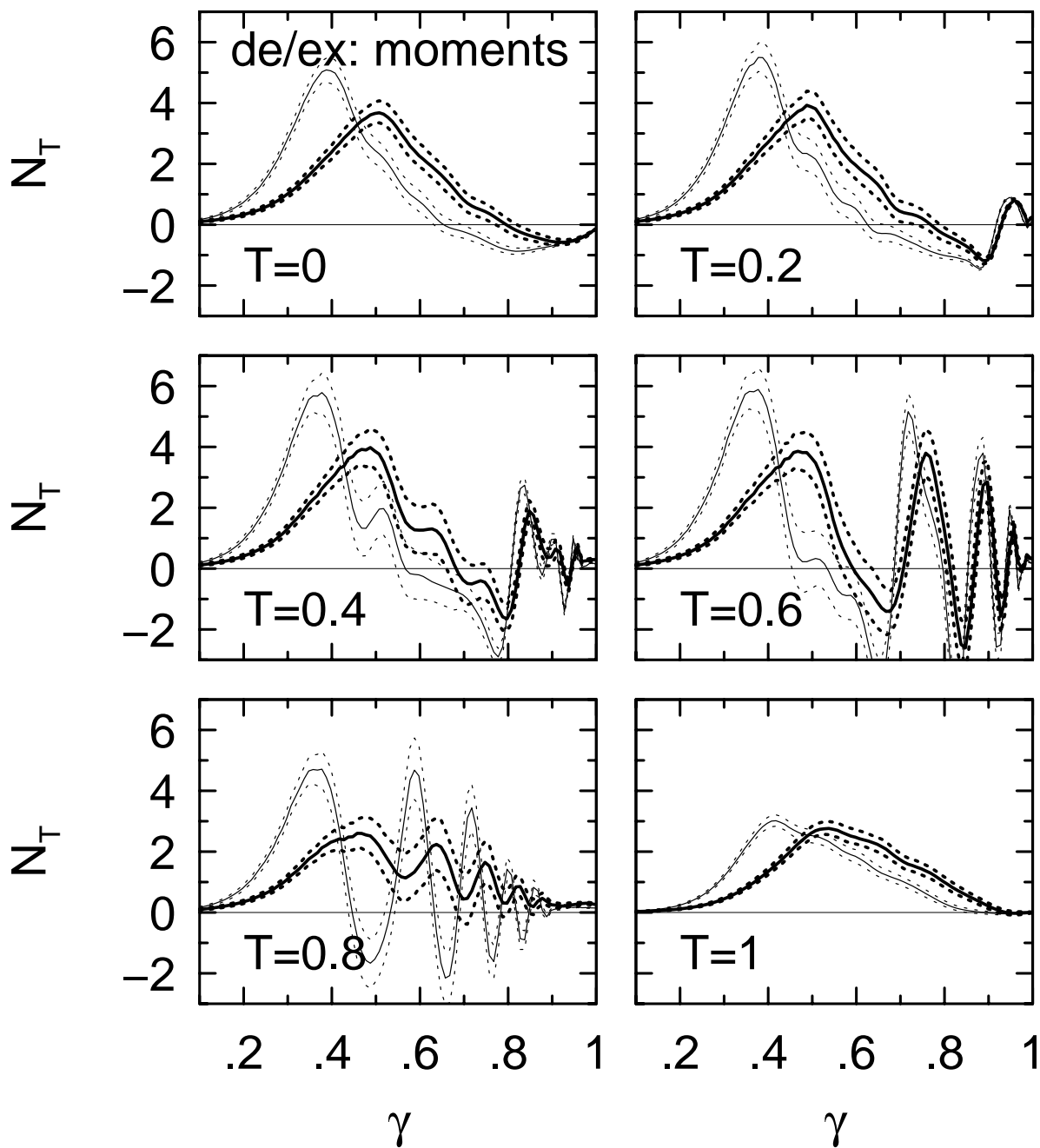


Fig. 7.— Distribution of intrinsic axis ratios for galaxies of profile type ‘de/ex’ ($0.5 < \text{fracDeV} \leq 0.9$), using the adaptive moments estimate of q . The heavy line is the distribution for galaxies with $M_r \leq -21.35$; the light line is for galaxies with $M_r > -21.35$. The dotted lines indicate the 98% confidence intervals, estimated by bootstrap resampling. The assumed value of the triaxiality T is given in each panel.

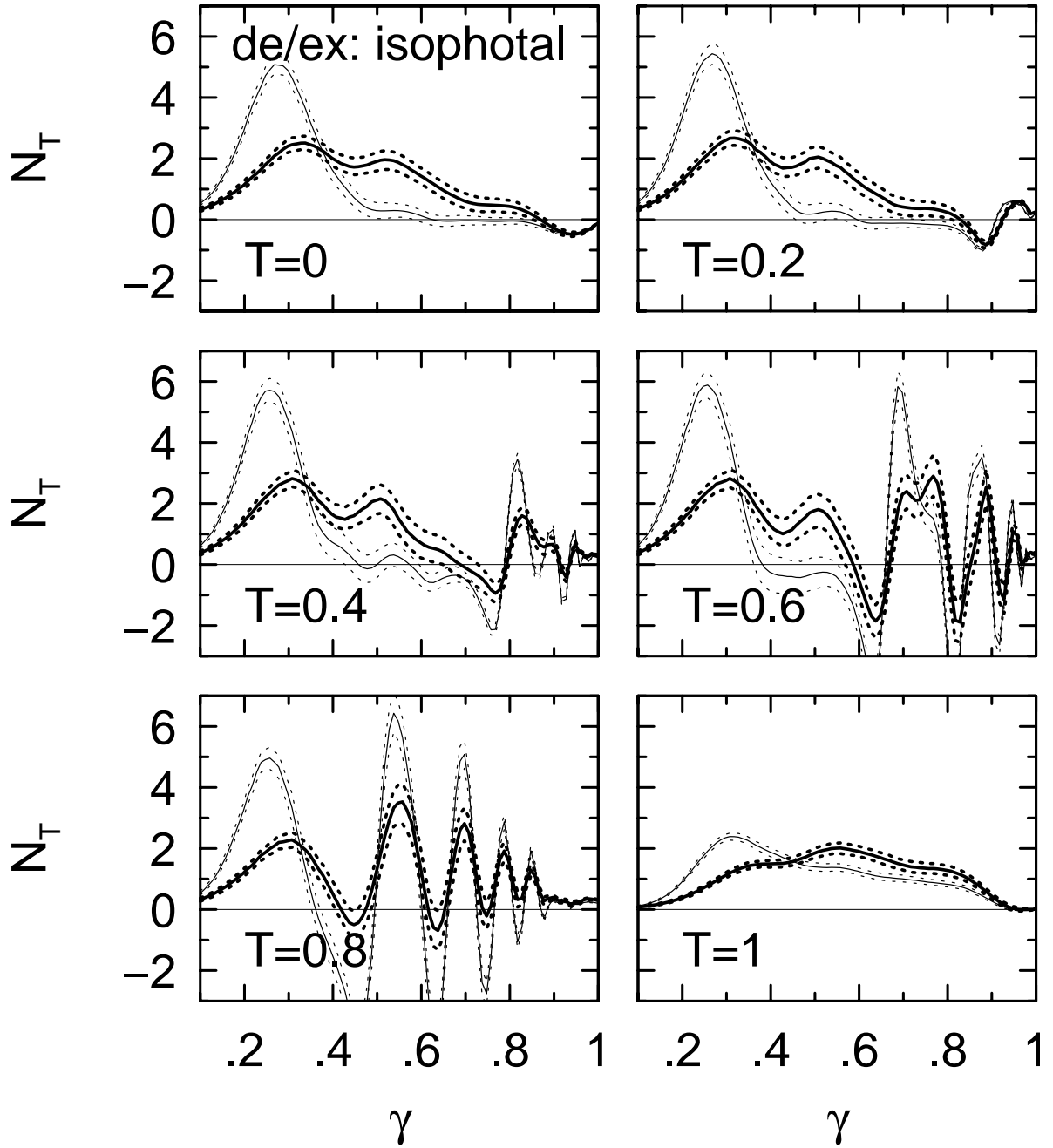


Fig. 8.— Same as Figure 7, but using the apparent axis ratio of the 25 mag/arcsec² isophote as the shape estimate.

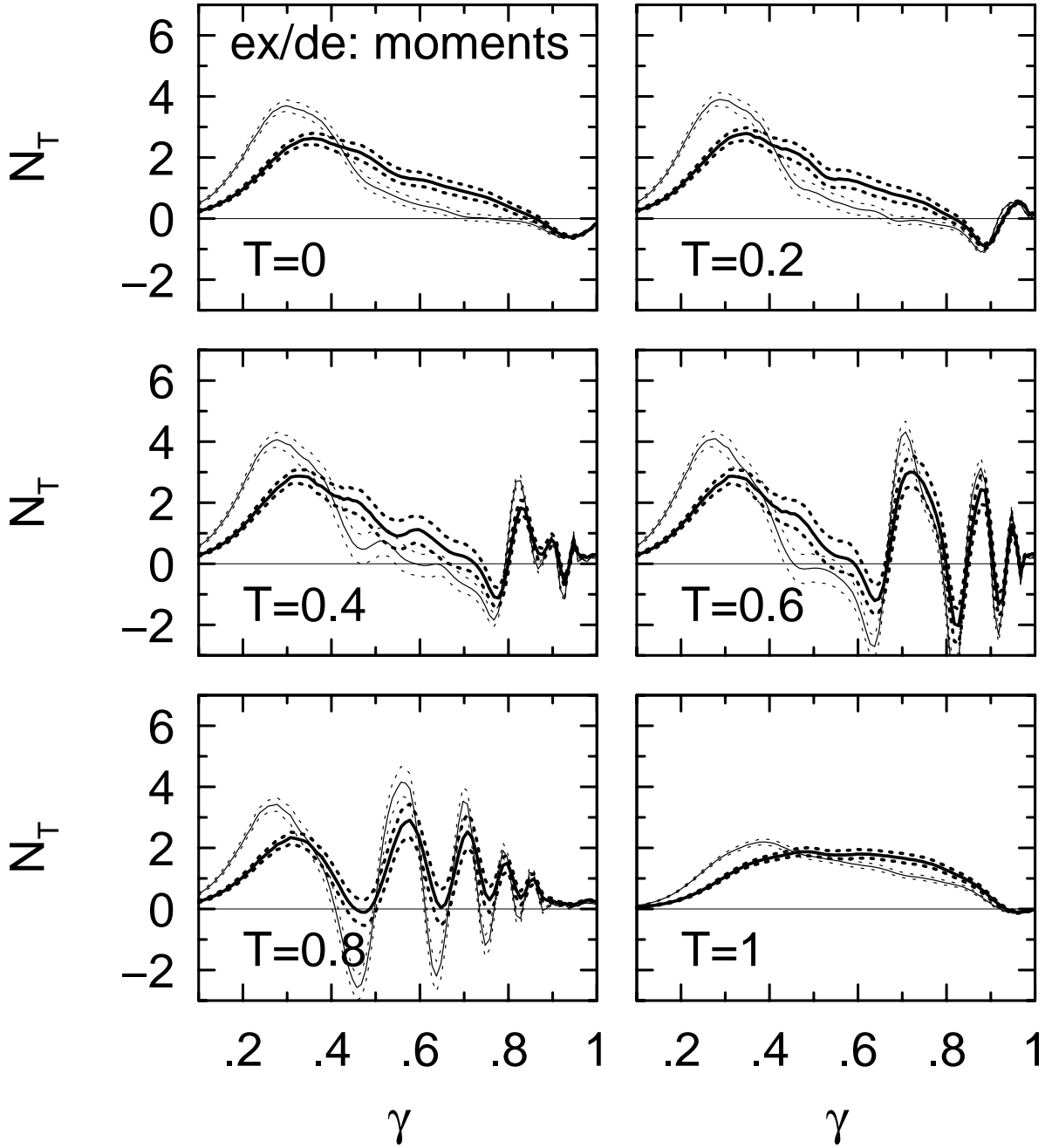


Fig. 9.— Distribution of intrinsic axis ratios for galaxies of profile type ‘ex/de’ ($0.1 < \text{fracDeV} \leq 0.5$), using the adaptive moments estimate of q . The heavy line is the distribution for galaxies with $M_r \leq -21.0$; the light line is for galaxies with $M_r > -21.0$. The dotted lines indicate the 98% confidence intervals, estimated by bootstrap resampling. The assumed value of the triaxiality T is given in each panel.

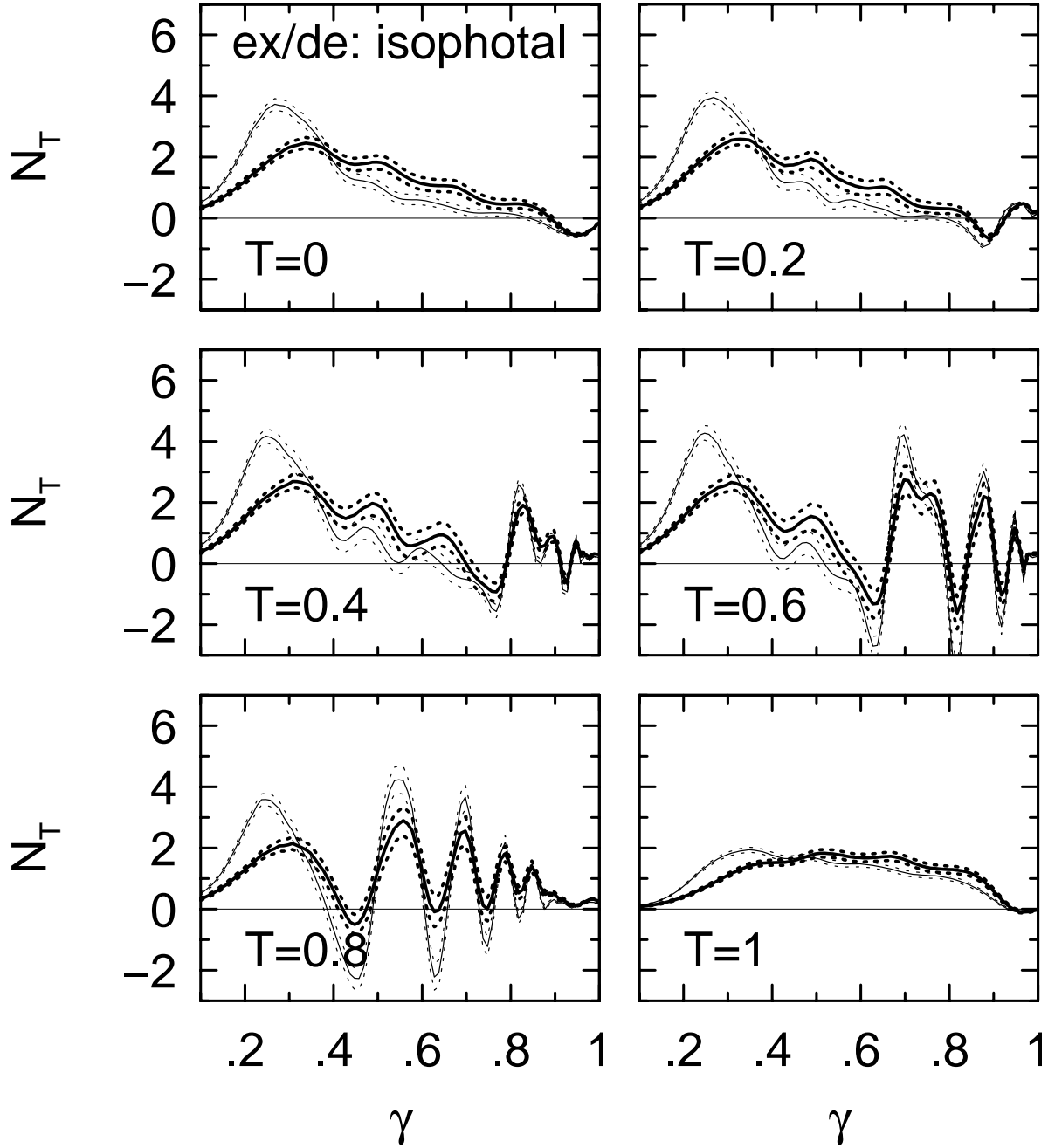


Fig. 10.— Same as Figure 9, but using the apparent axis ratio of the 25 mag/arcsec² isophote as the shape estimate.

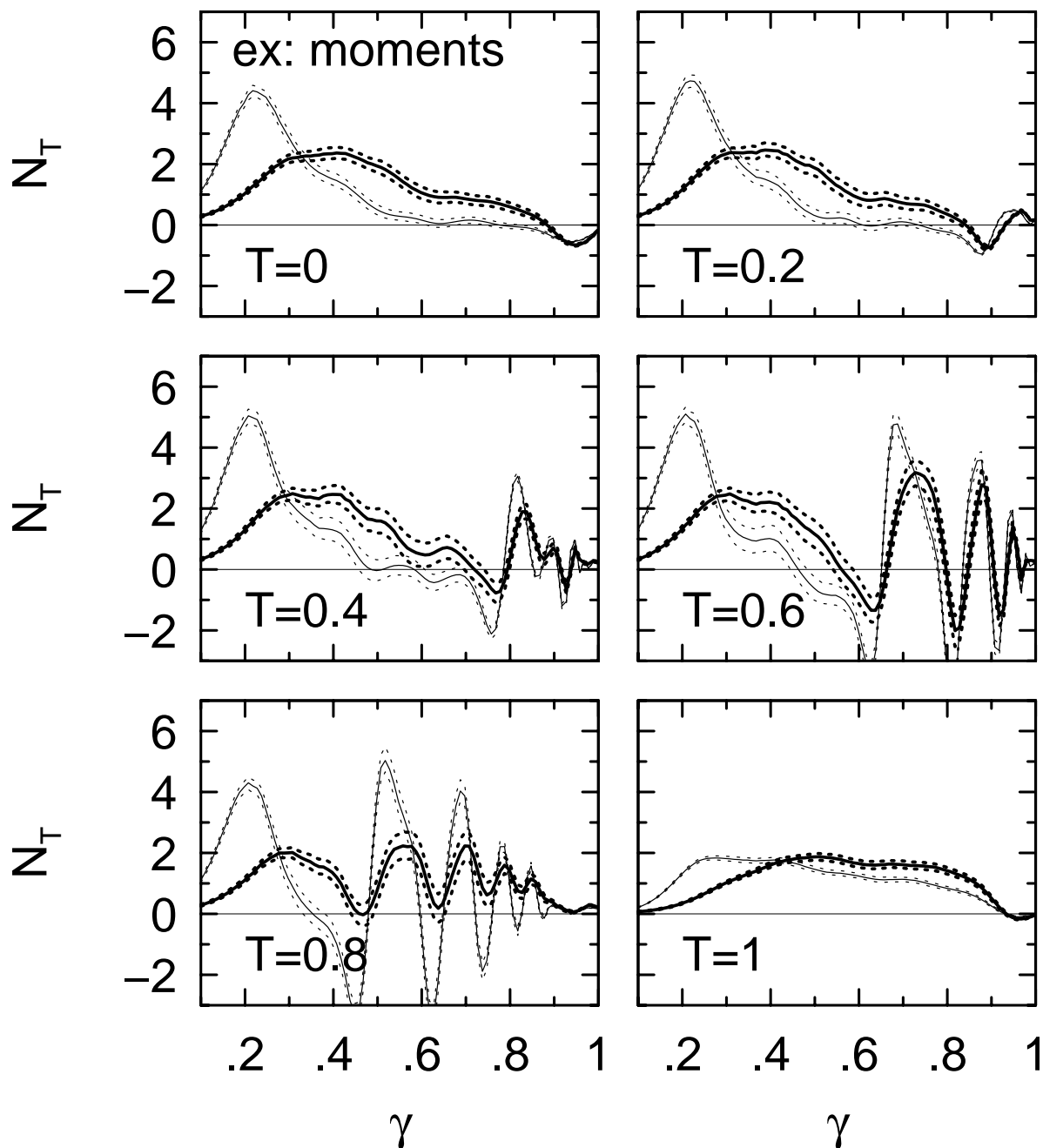


Fig. 11.— Distribution of intrinsic axis ratios for galaxies of profile type ‘ex’ ($\text{fracDev} \leq 0.1$), using the adaptive moments estimate of q . The heavy line is the distribution for galaxies with $M_r \leq -20.5$; the light line is for galaxies with $M_r > -20.5$. The dotted lines indicate the 98% confidence intervals, estimated by bootstrap resampling. The assumed value of the triaxiality T is given in each panel.

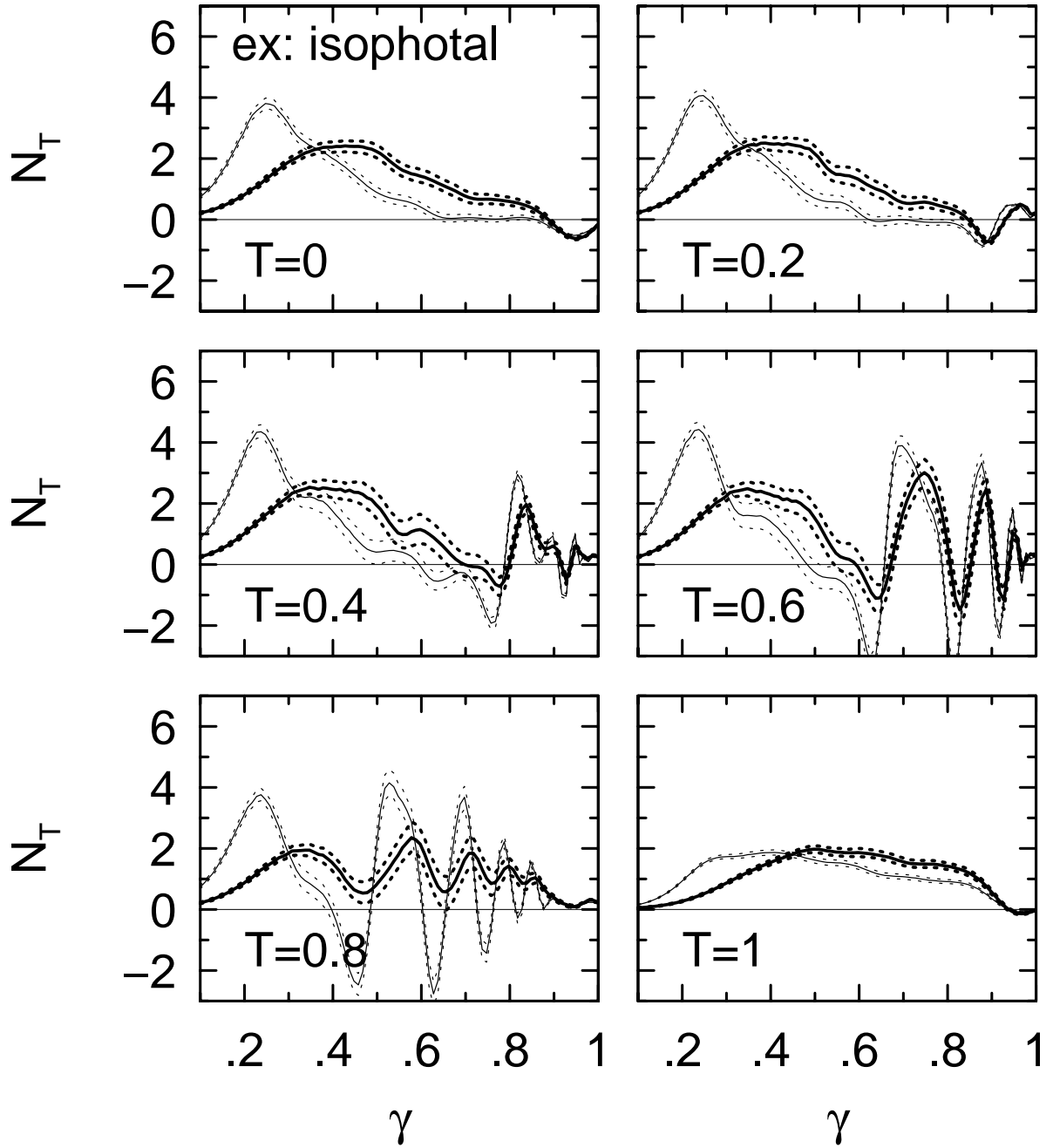


Fig. 12.— Same as Figure 11, but using the apparent axis ratio of the 25 mag/arcsec² isophote as the shape estimate.